Seismic Response of a Variable Cross-Section Shear Beam Building with Soil-Structure-Interaction

George D. Manolis & Athanasios A. Markou
Department of Civil Engineering. Aristotle University, Thessaloniki, GR-54124, Greece,
e-mail: gdm@civil.auth.gr & athanasiosmarkou@gmail.com

Petia S. Dineva
Institute of Mechanics, Bulgarian Academy of Sciences, 1113 Sofia, Bulgaria,
e-mail: petia @imbm.bas.bg

SUMMARY:
In here, we investigate the response of a cantilevered shear building to seismically induced ground motions in the presence of soil-structure-interaction phenomena. The novelty of the present approach lies in the representation of the variable stiffness of the structure using a distributed mass model that is exact in terms of the theory of elastodynamics. The ensuing modal analysis of the shear beam requires recovery of the system eigenmodes from the governing differential equation with non-constant coefficients in terms of a power series expansion. Next, the equations of the complete system comprising structure, foundation, surrounding soil plus a base isolator are combined in the frequency domain, yielding a non-symmetric matrix system. Upon solution in terms of frequency response spectra, the time response is reconstituted through use of the inverse Fourier transformation. Finally, a parametric study is conducted to investigate the influence of the surrounding soil and of the base isolator on the kinematic response of the structure.

Keywords: Seismic response; Distributed parameter systems; Soil-structure-interaction; Structural dynamics

1. INTRODUCTION

Soil-structure-interaction (SSI) occurs when there is a stiffness mismatch between structure and surrounding soil. In general, SSI comprises structural mechanics, geotechnical engineering and earthquake engineering (Kausel, 2010). As such, it requires specialized methods of analysis that can be classified as two major groups (Johnson, 1981): (a) sub-structuring techniques, whereby the problem is broken into its constituent parts, each solved by numerical and/or analytical methods, and the complete solution is assembled through use of continuity and equilibrium conditions at the common interfaces; (b) domain techniques, which invariably invoke use of the finite element method (FEM) to model the problem in its entirety including superstructure, foundation and surrounding soil (Bathe, 1982). In addition, the genesis and transmission of seismic signals from their source upwards to the surface where the structural system is located that has to be accounted for. Here, site effects play a prominent role in the modifications imparted to the seismic signals as they travel through soil deposits (Dineva et al., 2008). This in turn raises the open question of how to appropriately select seismic records and earthquake spectra (recorded or artificial) to be used as input in the analysis (Katsanos, 2010).

In this work, we develop an efficient hybrid technique, whereby the superstructure is modeled by its eigenproperties (Chopra, 1995), the surrounding soil by frequency dependent spring-dashpot-virtual mass coefficients (Mylonakis et al., 2002), while the foundation is assumed rigid and only its mass enters the picture. The advantage of the former representation is that we now use the exact model for the structural beam exhibiting shearing behavior in the presence of time-dependent loads. Furthermore, we treat a variable cross-section that implies non-constant material properties with height and allows for modeling dispersion phenomena as elastic waves travel upwards in the structure (Graff, 1975). We note here that it is possible to include flexural, axial and torsional modes of deformation that would cover a fully three-dimensional structural representation of a distributed mass system. Despite their advantage

of yielding exact representations of the dynamic response of continuous systems with obvious economy in the degree of model refinement required as compared to the FEM, distributed mass models have been used rather infrequently so far (Pan, 1992; Makris et al., 2010).

Finally, from a mechanics point of view, the presence of the surrounding soil is quite similar to a base-isolation (BI) system placed between the foundation and the superstructure (Naeim and Kelly, 2000). This allows for BI system of the lead rubber bearing type to be inserted in the same mechanical model as before, provided the bearings stiffness is modeled as a viscoelastic material with an equivalent initial stiffness parameter plus a relaxation constant for the aggregate effects of hysteresis-induced nonlinearities. This model, although rather simple unless the viscoelastic law involves fractional derivatives, is fully compatible with a frequency domain analysis (Atanackovic and Spasic, 2004).

The problem described above is now treated in three discrete steps. First, the influence of soft soil on the behavior of a typical mid-rise building of the shear-beam type is examined in terms of kinematic and inertia interaction effects. Next, a BI system is added comprising a nonlinear spring and its effect in the presence of SSI is gauged. Finally, the lack of uniformity with height in the structural stiffness is investigated for two basic cases, whereby the top story stiffness is 50% more/less than the base stiffness. Two input signals are used, namely white noise and synthetic ground motions that are calibrated against EC8 (2003) prescribed design spectra. The essence of this study is to examine the interplay of material and geometric parameters that influence key structural response variables in the presence of SSI.

2. DEVELOPMENT OF THE SSI-BI MODEL

As shown in Fig. 2.1(a), the SSI model comprises the superstructure, the rigid foundation, base isolator and surrounding soil, all modeled separately as discrete parameter systems with the exception of the superstructure, which for better accuracy is modeled as the distributed mass system of Fig. 2.1(b). We note that nonlinearities, such as those encountered primarily in the base isolator, are approximately modeled using viscoelasticity. Also, this shear type of structure is incapable of developing rocking motion due to base translation, which limits the model to 1D kinematics.

2.1. The Superstructure

The superstructure is modeled as a shear beam with distributed mass whose properties are listed in Table 3.1. The governing equation of motion in the presence of ground accelerations $\ddot{v}_G(t)$ at the base is given below, where $v(x,t)$ is the transverse motion of the shear beam:

$$GA_T\, \partial^2 v(x,t)\big/\partial x^2 = \rho A\left(\ddot{v}(x,t)+\ddot{v}_G\right) \tag{2.1}$$

The eigensolution for this beam with a fixed base and free boundary condition at the top (i.e., cantilever) is well known provided the beam has a constant cross-section with height. More specifically, the natural frequencies and the eigenvectors respectively are

$$\omega_n = \beta_n c_s = ((n+1)\pi/2L)c_S, \quad c_S = \sqrt{G/\rho}, \quad n = 0,2,4,6,... \tag{2.2}$$
$$\varphi_n(x) = \sin \beta_n x \tag{2.3}$$

where c_S is the speed of the shear wave travelling through the beam. Table 3.2 lists the values of the first four natural frequencies of the particular beam under consideration.

We now introduce modal decomposition for the superstructure by expressing the displacement in terms of the generalized coordinates $q(t)$ and the eigenvectors (Chopra, 1995) as follows:
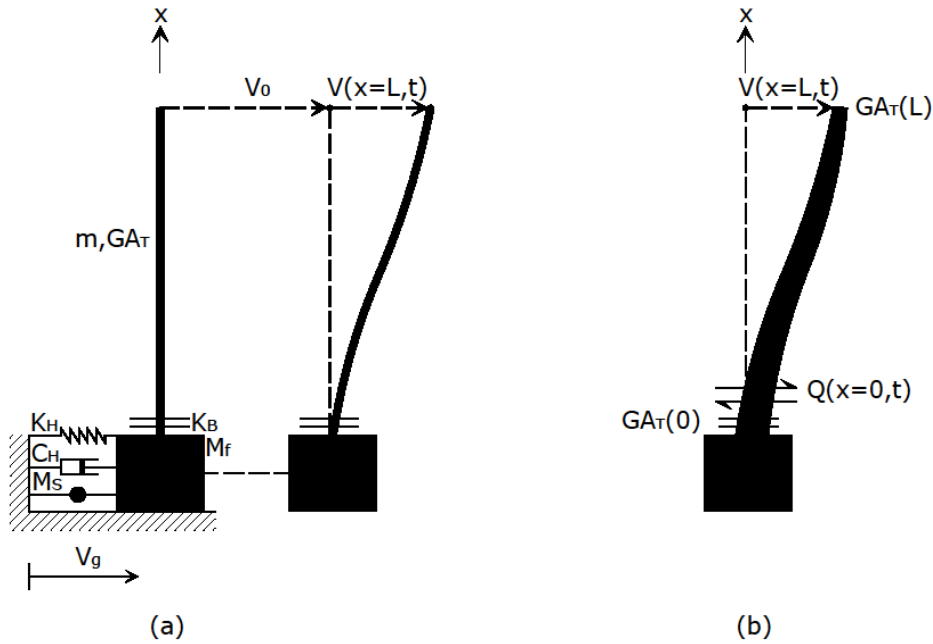
Figure 2.1. (a) The combined SSI mechanical system with (b) the structure as a shear-type cantilevered beam with a variable cross-section

$$v(x,t) = \sum_{n=1}^{\infty} \varphi_n(x) q_n(t) \tag{2.4}$$

Pre-multiplication of Eqn. 2.1 with the *m-th* eigenvector, integration over the length of the beam and use of the orthogonality property yields

$$M_n \ddot{q}_n(t) - K_n q_n(t) = -f_n^1 \ddot{v}_G(t) \tag{2.5}$$

as the governing equation for the fixed-base superstructure. The generalized mass, stiffness and forcing function in Eqn. 2.5 are given below respectively as

$$M_n = \rho_T \int_0^L [\varphi_n(x)]^2 dx, \quad K_n = G \int_0^L [d(\varphi_n(x))/dx]^2 dx, \quad f_n^1 = \rho_T \int_0^L [\varphi_n(x)] dx \tag{2.6}$$

In the above, $\rho_T = \rho/a$, $a = A/A_T$, where $a = 5/6$ is the shear factor correction for a rectangular cross-section of the beam.

2.2. The Soil-Foundation and Base Isolation Systems

Next, Table 3.3 lists all relevant properties for the soil-foundation system, which is modeled as an equivalent rigid disc of radius r resting on the elastic half-space (Reissner's solution) with the surrounding soil represented by a spring $K_H = 18.2Gr(1-v^2)/(2-v)^2$, a dashpot $C_H = 1.08\sqrt{K_H \rho_S r^3}$ and a virtual mass $M_S = 0.28\rho_S r^3$ element, which are practically frequency independent (Mylonakis et al., 2002). Regarding the rigid foundation, all we need is its overall

dimensions and mass density r, d, ρ_F, so that $M_F = \rho_F(\pi r^2 d)$. Since the fixed-end boundary conditions are already included in the eigenvalue problem, assembly of the SSI problem is simple, and achieved by imposing compatibility and equilibrium at the common interface. We note here that it is possible to add more degrees-of-freedom to the model so as to account for axial, torsional and flexural type of behavior, supplemented by the analogous soil elements.

The base isolation system considered is the lead rubber bearing (LRB) design (Naeim and Kelly, 2000). The constitutive law, for what is essentially a nonlinear spring element, is tri-linear with hysteresis, but this requires a time-stepping solution approach. In lieu of that, we start with a fractional derivative constitutive law (Atanackovic and Spasic, 2004), which relate the uniaxial stress and strain rates that develop in the LRB. This is expressed macroscopically as the following relation between BI restoring force F_L and lateral displacement w :

$$F_L(t) + \tau_F \ F_L^{(a)}(t) = K_L \{w(t) + \tau_W \ w^{(a)}(t)\}, \quad (.)^{(a)} = d^a(.)/dt^a \tag{2.7}$$

The derivative order appearing above is $0 \le a \le 1$, and the material constants must obey $\tau_W - \tau_F > 0$. For the purposes of this work, we use $a = 1$ and revert to linear viscoelasticity, whereby the LRB stiffness is modeled by a real part K_{L0} and a frequency-dependent imaginary part K_{L0}, η_L, with values given in Table 3.3.

2.3. Input motion

We first use a white noise type input, as shown in Fig. 3.1 (see also Table 3.4) to investigate the basic response of the combined SSI-BI system. Next, one could use synthetic ground motion acceleration input signals $\ddot{v}_G(t)$ generated by horizontally polarized shear (SH) waves reaching the soil-foundation interface. These signals are computed by accessing website *http://infoseismo.civil.auth.gr* that contains information developed through collaborative work (Dineva et al., 2008) on the transmission of seismic waves through complex soil stratigraphy. For instance, the signals reproduced in Fig. 3.2 show how a (fictitious) normalized, constant acceleration time signal is modified as it is filtered through a three-layered soil deposit with properties listed in Table 3.5. These types of signals can be further modified to take into account wave scattering effects caused by the presence of buried cavities and of both interface and internal geological cracks.

3. SOLUTION PROCEDURE

3.1. Frequency Domain Transformation

We first define the direct and inverse Fourier transforms (FT) as

$$U(\omega) = \int_{-\infty}^{\infty} u(t) \exp(-i\omega t) dt, \quad u(t) = (1/2\pi) \int_{-\infty}^{\infty} U(\omega) \exp(+i\omega t) d\omega \tag{3.1}$$

where ω (*rad/sec*) is the frequency. One reason for casting the SSI problem in the frequency domain is to include energy dissipation in the superstructure. This is achieved by using linear viscoelasticity, whereby complex-valued expressions are introduced for the stiffness parameters, with the imaginary part reproducing damping. The commonly used Kelvin (or structural damping) model is retained, yielding a shear modulus of the type $G = G_0(1.0 + i\omega\eta)$, where η the viscoelastic parameter and G_0 is the elastic stiffness (see Table 3.1). We note that the same basic type of viscoelastic model is also used for the base isolator.

Upon solution in the frequency domain, the inverse transformation to the time domain is accomplished numerically using the well-known fast Fourier transform (FFT) algorithm. Calibration of the algorithm is done using the white noise input of Fig. 3.1 of amplitude $U(\omega) = 0.01\,m$, while setting the frequency and time axes according to the values given in Table 3.4. More specifically, we start with the one-sided spectrum ($(\omega \geq 0)$ and use $N_H=256$ samples. The negative part of the spectrum is set equal to zero so that a total of $N=512$ sampling points are fed into the FFT algorithm. The inverse function is a point impulse centered at zero with peak value $I(0) = 2.05310\,m/\sec^3$, which upon multiplication with $2\Delta t = 2(0.025)\sec$ gives a $\ddot{u}(0) = 0.0102655\,m/\sec^2$ value that is sufficiently accurate (maximum error is 2.6%). A doubling of the half-sampling rate to $N=1024$ yields $\ddot{u}(0) = 0.0102257\,m/\sec^2$, which implies that the algorithm converges.
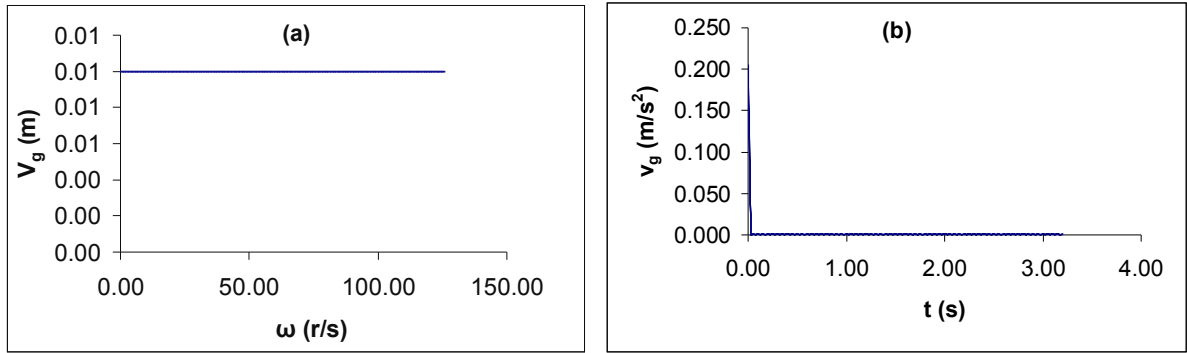
Figure 3.1. Incoming signals: (a) White noise amplitude $V_g(\omega)$ with (b) time domain real part $v_g(t)$
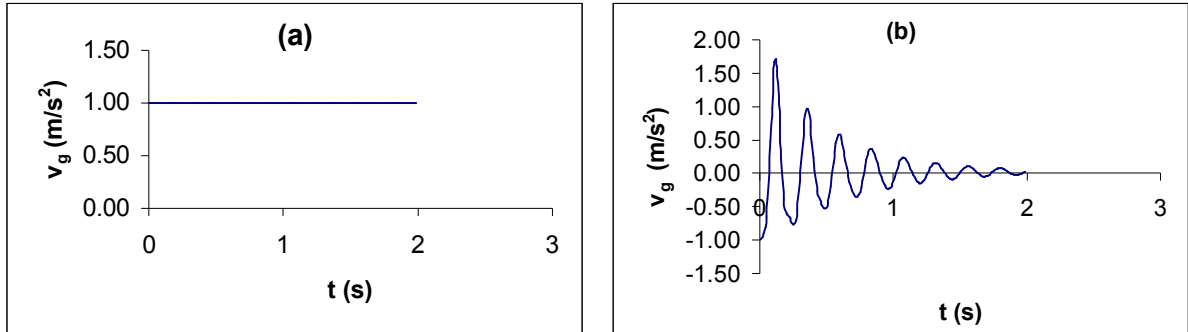
Figure 3.2. (a) Normalized SH-wave signal $v_g(t)$ and (b) filtered signal $v_g(t)$ through layered soil

3.2. The combined Structure-Soil-Foundation-Base Isolation Systems

In reference to Fig. 2.1, with $v_0(t)$ the motion at the foundation level, the coupled governing equations of motion for the combined SSI system are

$$M_n\,\ddot{q}_n(t) - K_n\,q_n(t) + f_n^1\,\ddot{v}_0(t) = -f_n^1\,\ddot{v}_G(t)$$
$$M_F\left(\ddot{v}_0(t) + \ddot{v}_G(t)\right) + C_H\dot{v}_0(t) + (K_H + K_L)\,v_0(t) = Q(0,t)$$

(3.2)

where $Q(0,t)$ is the base shear. Note that the rigidity of the foundation obviates the introduction of an additional degree-of-freedom to account for the base isolator. Next, given the uniaxial constitutive law for the shear stress as $\tau(x,t) = G\,\partial v(x,t)/\partial x$ and that $Q = A_T\,\tau$, we use the modal representation of

Eqn. 2.4 in the second of Eqs. 3.2 to get

$$M_F \ddot{v}_0(t) + C_H \dot{v}_0(t) + (K_H + K_L) v_0(t) - GA_T \sum_{n=1}^{\infty} (d\varphi_n / dx)\big|_{X=0} q_n(t) = -M_F \ddot{v}_G(t) \qquad (3.3)$$

The above equation is further processed by pre-multiplication with the *m-th* eigenvector, integration over the length of the beam and use of the orthogonality property. Combining this equation with the superstructure equation yields

$$[\bar{M}]\{\ddot{u}(t)\} + [\bar{C}]\{\dot{u}(t)\} + [\bar{K}]\{u(t)\} = -\{\bar{F}\}\ddot{v}_G(t); \{u\}^T = \lfloor q_1, q_2, q_3, ..., q_N, v_0 \rfloor \qquad (3.4)$$

where N is the total number of modes retained in the modal representation. Next, $[\bar{M}], [\bar{C}], [\bar{K}], \{\bar{F}\}$ are the modal mass, damping and stiffness matrices plus the forcing vector of the SSI system. We note that these matrices are non-symmetric because of the coupling effect and the off-diagonal terms involved are of the form

$$f_i^1 = \rho_T \int_0^L [\varphi_i(x)]dx, \quad f_i^2 = GA_T \{\sum_{n=1}^N \int_0^L [\varphi_n(x)]dx\}(d\varphi_i(x=0)/dx) \qquad (3.5)$$

Separate parametric studies have shown that *N=5* eigenvalues are sufficiently accurate to represent the superstructure. The final step is to transform the time-dependent governing matrix equations of motion to the frequency domain, so as to obtain the following coupled *6x6* system:

$$([\bar{K}] - \omega^2[\bar{M}] + i\omega[\bar{C}])\{U\} = -(i\omega)\{\bar{F}\}V_G(\omega); \{U\}^T = \lfloor \tilde{q}_1, \tilde{q}_2, \tilde{q}_3, \tilde{q}_4, \tilde{q}_5, \tilde{v}_0 \rfloor \qquad (3.6)$$

In the above, overbars in $\{U\}$ indicate the complex amplitude of the original time-dependent kinematic variables.

3.3. The Inhomogeneous Superstructure

We now examine the governing equation of motion, Eqn. 2.1, under free-vibration conditions $v(x,t) = V(x)\exp(i\omega t)$ and introduce a variable stiffness term $G(x) = \alpha(x)G_0$ so that

$$d\{\alpha(x)(dV(x)/dx)\}/dx + \beta^2 V(x) = 0, \quad \beta = \omega/c_S, \quad c_S = \sqrt{G_0/\rho_T} \qquad (3.7)$$

with homogeneous boundary conditions $V(0) = 0, dV(L)/dx = 0$. Assuming a linear variation of the dimensionless inhomogeneity term $\alpha(x) = 1 + \alpha_1 x$, Eqn. 3.7 becomes

$$(1 + \alpha_1 x)V'' + \alpha_1 V' + \beta^2 V = 0 \qquad (3.8)$$

where primes indicate derivatives with respect to *x*. We now seek a power series solution to the above differential equation as

$$V(x) = \sum_{K=0}^{\infty} p_K x^K, \quad V'(x) = \sum_{K=0}^{\infty} k p_K x^{K-1}, \quad V''(x) = \sum_{K=0}^{\infty} k(k-1)p_K x^{K-2} \qquad (3.9)$$

From the first of the boundary conditions, we recover the term $p_0 = 0$. Subsequent coefficients are obtained from the recurrence relation

$$p_K = -\{(k-1)/k\}\alpha_1 p_{K-1} - \{(k-2)!/k!\}\beta^2 p_{K-2} \tag{3.10}$$

for all $k \geq 2$ and with $p_1 = 1$. The eigenvalues β are computed directly from imposition of the second homogeneous boundary condition, i.e., $V'(L) = \sum_{K=0}^{\infty} k\, p_K L^{K-1} = 0$. Finally, by redefining for each computed eigenvalue β^J the corresponding power series terms as $p_K^J = p_K(p-1, \beta^J)$, we have the final form for the power series expansion

$$V(x) = \sum_{K=0}^{\infty} p_K^J x^K \tag{3.11}$$

The accuracy of the above power series solution was gauged against the homogeneous case of $\alpha_1 = 0$. It was found that a forty terms expansion produces accuracy reaching the fifth decimal place, but this accuracy is somewhat reduced as higher modes ($n > 4$) are computed.

3.4. Numerical Details

Given that the eigenvectors are no longer described by the closed form solutions of Eqn. 2.3, it is imperative to use numerical integration to compute the modal quantities in Eqn. 2.6 and 3.5. To that end, we employ Gaussian quadrature for the numerical integration of eigenvectors over the beam length as

$$\int_0^L f(x)\,dx = \int_{-1}^{1} f(x(\eta))\, J(\eta)\,d\eta, \quad \int_{-1}^{1} f(\eta)\,d\eta = \sum_{i=1}^{N} f(\eta_i) w_i \tag{3.12}$$

In the above, $f(x)$ is any eigenvector function, while (η_i, w_i) are Gauss points and weights and $J(\eta)$ is the Jacobian determinant of the transformation from the normalized interval $(-1 \leq \eta \leq +1)$ to the beam length ($0 \leq x \leq L$). For further accuracy, the beam length is subdivided into four sub-elements, while six-point Gaussian integration is performed within each sub-element. There is an additional complication that arises because the location of the Gauss integration points (a total of 24 points) does not match that of the discrete values for the eigenvector uniform sampling of 100 points. This problem is circumvented by introducing numerical interpolation by Lagrange's classical formula involving algebraic polynomials. This method was tested against exact integration of the homogeneous shear beam eigenvectors (i.e., sine functions) and proved to be extremely accurate.

Table 3.1. Dimensions-material properties of the superstructure with a being the measure of beam variability

L (m)	A (m²)	A_T (m²)	G_0 (kN/m²)	m (tn/m)	η (%)	α (m⁻¹)	α (m⁻¹)	α (m⁻¹)
20	4	3.33	11.67x10⁶	48	5	0	+0.0025	-0.0025

Table 3.2. N=4 eigenvalues for fixed-base shear beam superstructure with reference wave speed cs=2205(m/s)

	ω_1 (rad/sec)	ω_2 (rad/sec)	ω_3 (rad/sec)	ω_4 (rad/sec)
α=0	77.44	232.30	387.20	542.10
α=-0.0025	70.90	199.99	331.86	526.86
α=+0.0025	82.64	257.31	402.45	644.31

Table 3.3. Material properties of the soil-foundation-base isolation sub-systems

μ (kN/m²)	ν	ρ_S (tn/m³)	ρ_F (tn/m³)	R (m)	D (m)
27,000	0.25	2.1	2.4	3	1
M_F (tn)	M_S (tn)	K_H (kN/m)	C_H (kN sec/m)	K_{L0} (kN/m)	η_L (%)
67.85	15.87	451,286	5,463	20,000	25

Table 3.4 . Frequency and time domain scales and white noise input signal characteristics

Ω (rad/sec)	$\Delta\omega$ (rad/sec)	T (sec)	Δt (sec)	$V_g(\omega)$ (m)	$v''_g(t)$ (m/sec^2)	N
125.664	0.9817	3.2	0.025	0.001	0.00102655 δ(t-0)	512

Table 3.5. Three layered soil profile stiffening with increasing depth from surface (overall soil damping is 7%)

Layer height h (m)	10	20	30
Layer wavespeed c_S (m/sec)	300	600	900
Layer density ρ (tn/m^3)	2.0	2.1	2.2

Following solution of Eqn. 3.6 that yields the generalized coordinates, the shear beam displacement at the top $v_1 = v(L,t)$ can be synthesized according to Eqn. 2.4, and the base shear forces $Q_0 = Q(0,t)$ can then be computed using elementary beam theory. A final step would be to compute energy measures from the motion imparted to the superstructure from the base motion, which would give a good indication of the damages expected, but is the subject of future work.

4. NUMERICAL RESULTS

4.1. Calibration of the Superstructure model

In this section, we first calibrate the distributed parameter model by examining the influence of the inhomogeneity parameter α in the absence of any SSI effects. More specifically, Table 3.2 completes the picture by listing the first four eigenvalues when the fixed-base cantilever beam is inhomogeneous, i.e., for cases $\alpha = 0, 0.025, -0.025$ that respectively correspond to $G(x) = G_0$, $G(L) = 1.5G_0$, $G(L) = 0.5G_0$. We observe that an increase in stiffness with height is clearly reflected in higher numerical values for the natural frequencies, and that the spread between inhomogeneous and homogeneous cases values becomes more pronounced for higher modes.

4.2. Numerical Results for SSI

The numerical results of the parametric SSI study are now collected in Fig. 4.1 and 4.2. More specifically, both figures plot top story and ground level displacements for an incoming white noise signal, presented in terms of frequency amplitudes and real parts of the time response. In the presence of SSI, Fig. 4.1 first examines the effect of structural damping in the superstructure (see Table 3.1) and also that of a base isolator (see Table 3.3). Similarly, Fig. 4.2 examines the effect of beam inhomogeneity (see Table 3.2) in the presence of SSI.

In the former case, we observe that structural damping is clearly beneficial in reducing the top story displacement, but leaves the base displacement virtually unaffected. Base isolation, on the other hand, is beneficial in both cases as it essentially blocks the transfer of a certain amount of seismic energy to the entire superstructure block. The amount of motion reduction for BI is, roughly speaking, about 50% in the frequency plots, but translates to smaller reductions in the transient signals that die out quite rapidly for this type of seismic input.

Finally, inhomogeneity results in both amplitude changes and natural frequency shifts for the superstructure in the presence of SSI. As expected, the frequency amplitude plots move to the right as the cantilever stiffness increases with height, while the opposite is true for the cantilever with decreasing stiffness. The amplitude itself increases in the former case and decreases in the latter case, indicating that a top-heavy structure will experience more motion at the top compared to one that is correctly tapered. This, in turn, is clearly visible in the corresponding time history plots.
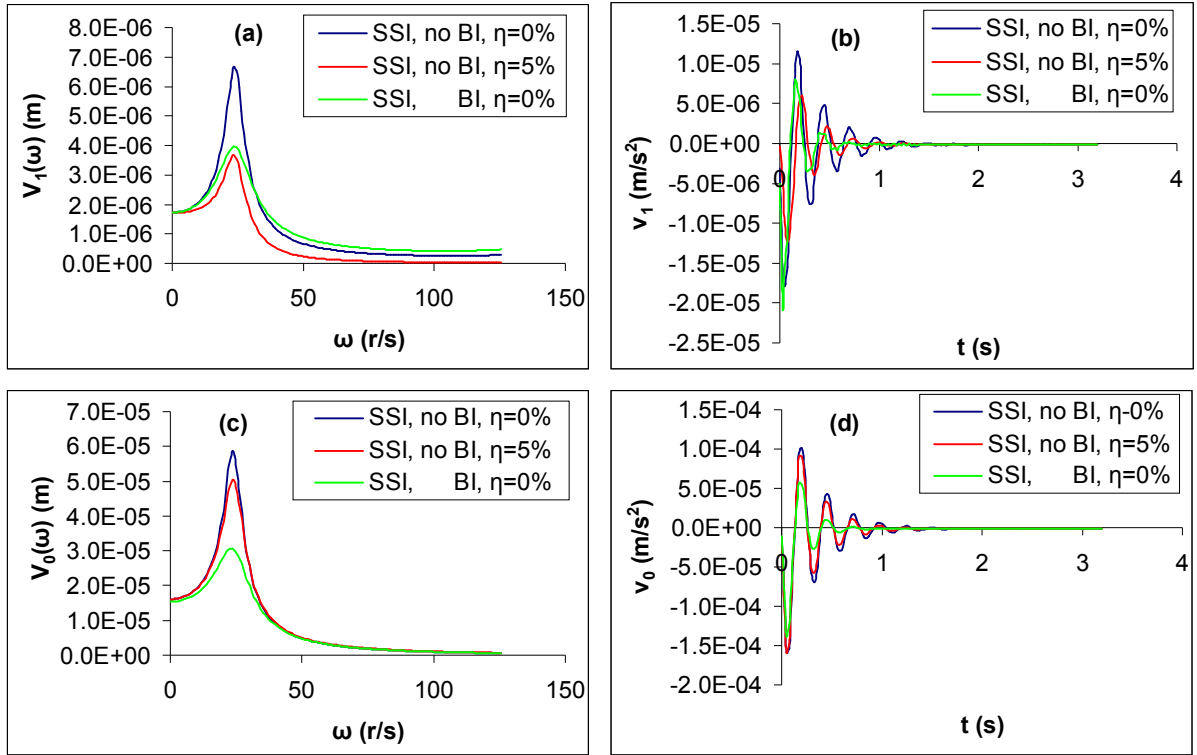
Figure 4.1. SSI response of homogeneous cantilever to white noise input: (a) Top story displacement amplitude $V_1(\omega)$ and (b) time domain real part $v_1(t)$; (c) Ground level displacement amplitude $V_0(\omega)$ and (d) time domain real part $v_0(t)$ in the presence of structural damping (η) and BI (K_{L0}, η_L)
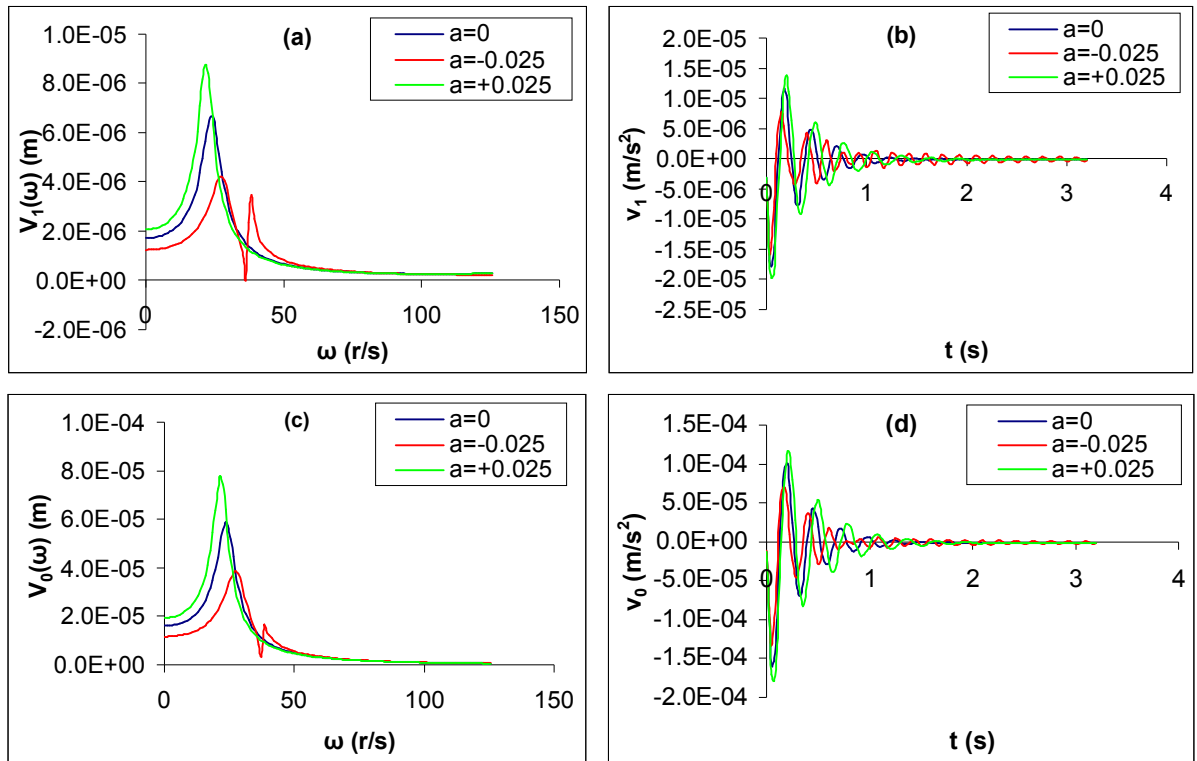
Figure 4.2. SSI response of inhomogeneous cantilever to white noise input: (a) Top story displacement amplitude $V_1(\omega)$ and (b) time domain real part $v_1(t)$; (c) Ground level displacement amplitude $V_0(\omega)$ and (d) time domain real part $v_0(t)$ when $\alpha=0$, $\alpha=-0.025$, $\alpha=+0.025$

5. CONCLUSIONS

In this work, we investigated the influence of the surrounding soil on the seismic response of a stiff cantilevered structure of the shear-beam type as a first step in determining the potential for damage, as a function of incoming seismic signal strength. The relevant comparison was between the fixed-base, constant-cross section case, and the complete SSI model with base isolation and variable structural cross-section. The present formulation allowed for economy in the mechanical modeling procedure as compared to the use of large scale finite element programming, which requires a considerable detail in the representation of the surrounding soil. Additional items that have to be accounted for is the introduction of a fully 3D structural behavior that encompasses flexural, torsional and axial modes of vibration, plus the use of an advanced constitutive law based on fractional derivatives to model the base isolator.

In sum, a structure in the presence of SSI and with a BI system will perform differently as compared to the case where the structure is founded on competent soil and/or rock, for two basic reasons: (a) there is filtering affecting the input ground motion signal at the base of the structure, and (b) the overall mechanical characteristics of the combined structural system have changed as compared to the original structure resting on firm ground. Thus, a BI design has to account for SSI in order to have the system fine-tuned to the particular geological conditions and seismicity of the building site in question.

REFERENCES

Atanackovic, T.M. and Spasic, D.T. (2004). On viscoelastic compliant contact-impact models. *Journal of Applied Mechanics* **71:1**, 134-139.

Bathe, K.J. (1982). Finite Element Procedures in Engineering Analysis. Prentice-Hall, Englewood Cliffs.

CEN Eurocode 8 (2003). *Design of Structures for Earthquake Resistance. Part 1: General Rules, Seismic Actions and Rules for Buildings.* European Committee for Standardization, Brussels, Belgium.

Chopra, A.K. (1995). Dynamics of Structures, Pearson Prentice Hall, Englewood Cliffs.

Dineva, P.S, Manolis, G.D. and Rangelov, T.V. (2008). Site effects due to wave path inhomogeneity by BEM. *Engineering Analysis with Boundary Elements* **32:12**, 1025-1036.

Graff, K. (1975). Wave Motion in Elastic Solids, Ohio State University Press, Columbus.

Johnson, J.J. (1981). *Soil-Structure-Interaction: The Status of Current Analysis Methods and Research.* Nuclear Regulatory Commission Research Report NUREG CR-1780,Washington, DC.

Katsanos, E.I., Sextos, A.G. and Manolis, G.D. (2010). Selection of earthquake ground motion records: A state-of-the-art review from a structural engineering perspective. *Soil Dynamics and Earthquake Engineering* **30:4**, 157-169.

Kausel, E. (2010). Early History of Soil-Structure-Interaction. *Soil Dynamics and Earthquake Engineering* 30:9, 822-832.

Makris, N., Kampas, G. and Angelopoulou, D. (2010). Modal Analysis of Isolated Bridges with Transverse Restraints at the End Abutments. *Proceedings of the 9th HSTAM International Congress on Mechanics.* Edited by P. Papanastasiou et al.*,* Limassol, Cyprus, 12-14 July 2010, 705-712.

Mylonakis, G., Gazetas, G., Nikolaou, S. and Chauncey, A. (2002). *Development of Analysis and Design Procedures for Spread Footings.* MCEER Report No. 02-0003, State University of New York at Buffalo, New York.

Naeim, F. and Kelly, J. M. (2000). Design of Seismic Isolated Structures: From Theory to Practice, CRC Press, Boca Raton, Florida.

Pan, T.C. (1992). Dynamic characteristics of base-isolated shear buildings. *Proceedings of the 10th World Conference on Earthquake Engineering.* Balkema, Rotterdam, 2509-2514.